

## Evaluation of Flow and Solute Transport Parameters for Heap Leach Recovery Materials

David L. Decker\* and Scott W. Tyler

### ABSTRACT

Mining low-grade precious metals deposits often involves the bulk processing of ore by leaching with cyanide. Once the precious metals concentration in the leachate fluid drops to an economic cutoff point, processing ceases and the mine is required to meet drinking water standards for the latent leachate fluid that continues to drain from the heap. A common closure method is to rinse the heap with relatively clean water until the those requirements are met. However, it has been observed that concentrations of constituents, cyanide in particular, remain elevated at rinse times that exceed those times predicted with a simple advective-dispersive type of transport model. To quantify the flow and transport behavior of spent heaps, the hydraulic and solute transport characteristics of several heap-leach materials from northern Nevada have been determined. Data from the U.S. Bureau of Mines laboratory column tracer tests and new data collected from a series of tracer experiments with sodium  $\text{Br}^-$  on heap material collected from the a large-scale heap in the Carlin Trend, Elko County, Nevada, are presented. A 6-m scale column incorporating time domain reflectometry was used to investigate the rinsing characteristics of spent heap-leach material. The breakthrough curve data from these experiments are analyzed using the traditional advection-dispersion equation and a dual-porosity model. The dual-porosity model provided significantly improved fits to the observed data compared with the advection-dispersion model. Data from the experimental results are used to show optimal rinsing strategies can be developed when heap hydraulic properties are considered.

**T**HE state of Nevada is the largest producer of gold and silver in the USA. In 1996, the precious metals mines in Nevada produced >7 million troy ounces of gold and 20 million troy ounces of silver (NBMG, 1997).

Desert Research Inst., Water Resources Center, University and Community College System of Nevada, 2215 Raggio Parkway, Reno, NV 89512-1095. Received 23 Jan. 1998. \*Corresponding author (decker@dri.edu).

Published in J. Environ. Qual. 28:543-555 (1999).

A large percentage of this production is derived from heap-leach processing of ore mined from open pits. Heap-leach processing involves the placement of ore onto engineered impervious liners. The scale of a typical heap can range from a few hectares to many hundreds of hectares in surface area, and up to 100 m in height. To remove the metals, cyanide is introduced at the top of the heap through overhead or drip irrigation methods. Cyanide has a strong affinity for most metals, and is capable of leaching them from the ore mass. Once the product metal concentration has fallen below an economically mineable cutoff point, production ceases, and the heap must be closed. To do so requires meeting the federal drinking water standard for cyanide (0.20 mg/L weak acid dissociable [WAD]) in the effluent stream at the bottom of the heap. Though cyanide is a cost effective leaching agent from a heap production economics standpoint, cyanide is also toxic to animals and people. Therefore, it is desirable to limit the release and exposure of cyanide to the environment during both heap production and, in particular, after closure. To better understand the mechanisms of cyanide transport in a heap, this paper focuses on the physics of solute transport in heap materials.

In Nevada, the most common method of rinsing cyanide from spent heaps is to irrigate the top of the heap with clean water until the leachate water cyanide concentration meets the closure requirement, at which time the rinse water is turned off. However, it has been observed that if another measurement of cyanide is made from several days to months later, the concentration is often elevated significantly above the level reached

**Abbreviations:** WAD, weak acid dissociable; ADE, advection-dispersion equation; USBM, U.S. Bureau of Mines; EC, electrical conductivity; TDR, time domain reflectometry.

during rinsing. The apparent immobility of cyanide during rinsing is problematic to both the actual rinsing of cyanide from the heap, and to estimating the economics of heap detoxification. In an effort to develop a method of determining heap rinse performance, this study has evaluated the flow and transport characteristics of several heap leach materials using two conceptual modeling approaches: advection–dispersion transport, and transport through a dual-porosity medium. The objective of this work is to develop an understanding of the physics of transport in mine heap structures with the goal of numerically simulating cyanide rinse behavior for the purpose of formulating efficient, cost effective rinse strategies that will limit the long-term environmental impact.

A number of mining engineering studies have been performed that focus on the rinsing of cyanide from spent heap-leach operations (Dix et al., 1992; Comba et al., 1992; McClelland, 1991; Schafer and Van Zyl, 1991). McClelland (1991) performed a laboratory scale cyanide leaching and rinsing experiment. These results indicated that most of the mass of cyanide was removed after three pore volumes had been rinsed through the column, but that the cyanide concentration did not fall below 0.20 mg/L until after throughput of 15 pore volumes. Dix et al. (1992) completed laboratory scale column experiments on a variety of heap materials. This study conducted cyanide rinse evaluations using cyanide with chloride as a conservative tracer. These workers based preliminary conclusions on the time and volume of water required to rinse a solute out of a column to a limit of 0.20 mg/L. A solute transport parameter analysis of these data are presented in this paper.

Additional studies have been carried out on spent heap-leach pads. Comba et al. (1992) performed a field-scale cyanide degradation and detoxification study at a spent silver production heap. Schafer and Van Zyl (1991) also examined the natural breakdown of cyanide in a spent heap. These studies focused primarily on quantifying the natural cyanide degradation processes but did not examine the field-scale hydrology of the heaps studied.

Two studies have been completed by Murr et al. (1981) and Cathles and Murr (1980) that used a very large column to examine leaching efficiencies of copper-bearing ore. A 3.1 m diameter by 10.8 m high column filled with ore was used to evaluate the effects of particle-size distribution, rock dissolution during leaching, flow channel size and location, and column permeability on leaching efficiency. They found that permeability and flow field distribution were critical to understanding the hydraulic behavior of the column. Though these studies were focused on the economics of heap-leaching of copper ore, they set a precedent for exploring the hydraulics of water transport in heap-leach recovery operations.

Dixon (1992) proposed a flow and transport model that is similar to the dual-porosity model proposed by Parker and van Genuchten (1984). However, the study assumes that dispersion does not occur in the mobile water phase, and that water moves strictly by a piston

displacement mechanism. This study did not show that the proposed model was a significant improvement over the advection–dispersion transport model.

## SOLUTE TRANSPORT IN POROUS MEDIA

The mathematical formulation of solute transport in porous media is based on the principles of conservation of mass and energy. The simplest formulation of solute transport is the advection–dispersion equation (ADE). The ADE is suitable for a homogeneous medium and can be used to simulate reactive transport involving more than one solute. The dual-porosity (or multiregion) model of Parker and van Genuchten (1984) accounts for heterogeneity through a mass transfer function between relatively low and high permeability zones. Parker and van Genuchten (1984) considered the flow domain to consist of a mobile water region and a second, immobile region. Dual-porosity models are most often used to model solute flow in fractured systems, where the low-permeability zone is the rock matrix, and the high-permeability zone is the fracture. However, these models may be of value in modeling solute transport in a heterogeneous heap.

### Dual-Porosity Transport Model

In a locally unsaturated, dual-porosity medium, the total volumetric water content can be considered to be the sum of the volumetric water content that is mobile,  $\theta_m$ , and the volumetric water content that is immobile,  $\theta_{im}$ :

$$\theta = \theta_m + \theta_{im} \quad [1]$$

The governing equations for the dual-porosity model can be described by incorporating terms for both the immobile and mobile phases into the ADE:

$$(\theta_m) \frac{\partial C_m}{\partial t} + (\theta_{im}) \frac{\partial C_{im}}{\partial t} = \theta_m D_m \frac{\partial^2 C_m}{\partial x^2} - q \frac{\partial C_m}{\partial x} \quad [2]$$

where  $C_m$  is the solute concentration in the mobile, or advective, capable zones,  $C_{im}$  is the solute concentration in the dead-end pore spaces or low-permeability zones,  $q$  is the advective flux rate, and  $D_m$  is the dispersion coefficient. Note that when  $\theta_{im} = 0$ , Eq. [2] reduces to the traditional one-dimensional advection–dispersion equation (Parker and van Genuchten, 1980). This dual-porosity model assumes that there is no advective component to solute transport in the immobile fraction. Advective transport occurs only in the mobile phase. The rate of change of the immobile phase concentration with time is assumed to be dependent on a first-order mass transfer coefficient that describes the rate of mass exchange between the mobile and immobile phases as:

$$(\theta_{im}) \frac{\partial C_{im}}{\partial t} = \alpha^* (C_m - C_{im}) \quad [3]$$

Equations [2] and [3] are the coupled partial differential equations that govern dual-porosity flow in the dual-porosity numerical flow and transport model used in this study, CXTFIT (Parker and van Genuchten, 1984), and is mathematically similar to that originally formu-

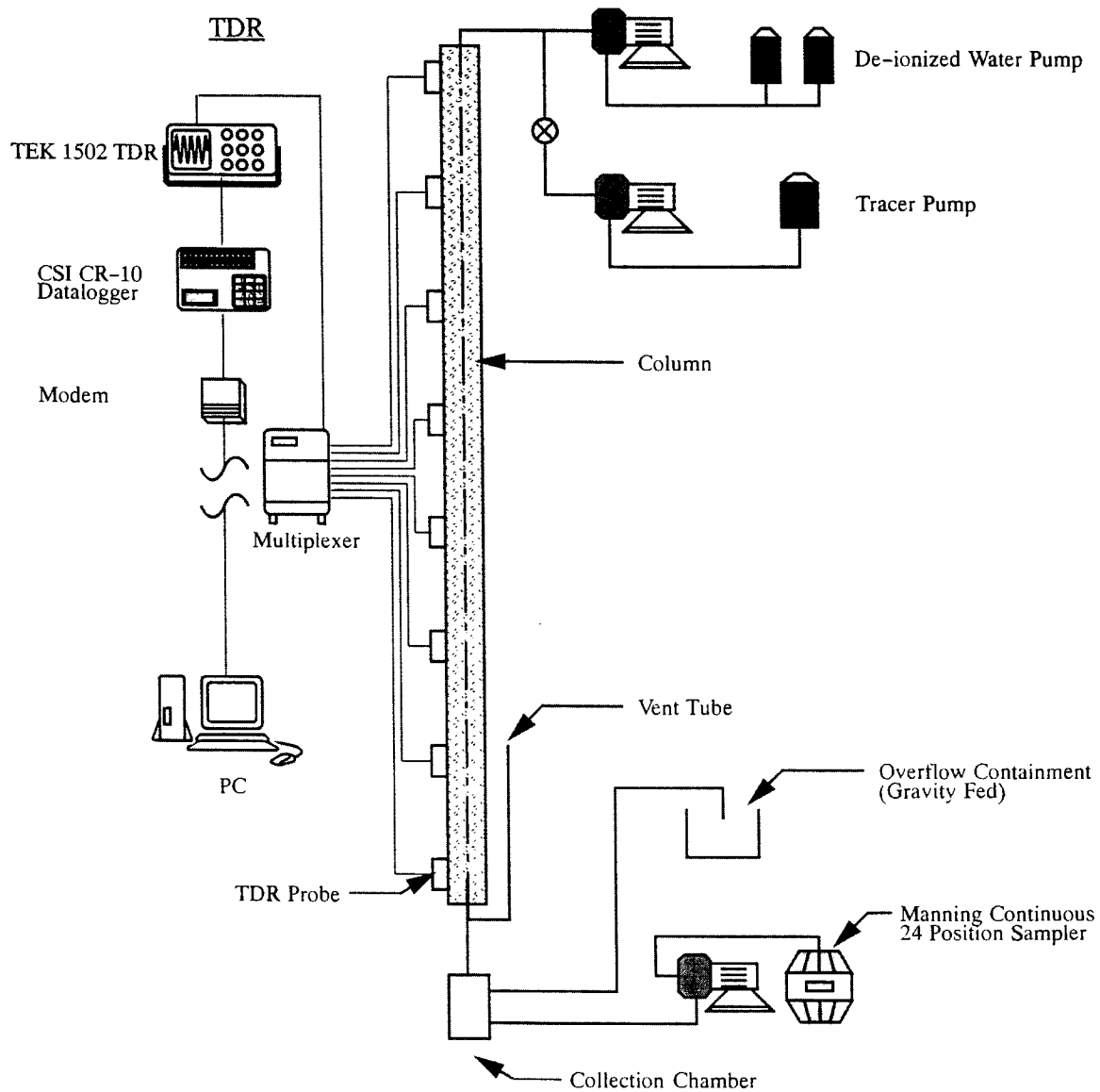


Fig. 1. Six-meter column experiment schematic. The TDR probes and associated electronics are shown on the left side of the schematic, while the hydraulic and fluid collection systems are shown on the right.

lated to address petroleum reservoir flow and transport problems (Coats and Smith, 1964).

## METHODS AND MATERIALS

### U.S. Bureau of Mines Experiments

The U.S. Bureau of Mines (USBM) conducted column cyanide rinse and tracer experiments on a variety of heap materials (Dix et al., 1992). The columns were Plexiglas tubes 15 cm in diameter and 122 cm long. Ore was packed into each column with an external vibration source during the initial filling. A Buchner funnel filled with 0.6 cm diameter gravel was used at the bottom of the columns as a filter pack. Fluid was admitted into the top of a column through plastic tubing and a positive displacement pump, and the outfall was collected through a gravity drainage system for analysis and disposal.

The USBM used NaCl as a tracer, with concentrations up to 260 000 mg/L  $\text{Cl}^-$  (2.7 m NaCl) with pulse durations up to 55 min in length. Tracer and deionized water rinse application rates were determined from rinse rates used during the rinse

of the field-scale heap by the mine operator. During NaCl tracer experiments, an inline electrical conductivity (EC) meter was used to collect continuous EC data for subsequent breakthrough curve development. During cyanide rinse studies, a discrete fluid sample was taken at regular intervals for laboratory analysis of WAD cyanide.

### 6 m Scale Column Experiments

The containment vessel used in the column experiment consisted of four 1.5 m tall sections of 20.3 cm diameter PVC schedule 40 pipe. The individual sections of the pipe were bolted together using flange fittings glued to the ends of the pipe and a rubber gasket between the flanges was used to seal the joint. The bottom end of the lowest section of pipe was sealed with a PVC end cap into which a plastic tube was installed to permit drainage. The top of the column was completed using a removable slip cap into which a plastic tube was installed to connect the water supply pump to the column (Fig. 1).

Three pumps were used to deliver fluid to and from the

**Table 1. Hydraulic retention function fitted and measured parameters.**

| Parameter                                                 | Value               |
|-----------------------------------------------------------|---------------------|
| Residual water content, $\theta$ ,                        | $0.07 \pm 0.02$     |
| Saturated water content, $\theta_s$ ,                     | 0.41                |
| $n$                                                       | $3.25 \pm 1.92$     |
| $\alpha$ , $\text{cm}^{-1}$                               | $0.0478 \pm 0.0612$ |
| $L$                                                       | $-2.70 \pm 0.91$    |
| Saturated hydraulic conductivity, $\text{cm/h}$ , $K_s$ , | $4.77 \pm 0.53$     |

column. A positive displacement diaphragm pump was used to deliver deionized water to the top of the column. This pump was calibrated in place for the desired flow rate before the start of each experiment. In addition, the solute delivery was accomplished with a peristaltic pump that was likewise calibrated to the desired flow rate before the start of each experiment. Fluid was collected at the bottom of the column by gravity drainage and was delivered to a Manning sampler for outfall water sample collection.

The column was instrumented with eight three-wire time domain reflectometry (TDR) probes. Each of the four sections of the column had two sets of probes installed. To install the TDR probes into the column body, holes were drilled at the same spacing as the TDR probe rods into each column section so that the plane created by the probe rods was perpendicular to the long axis of the column.

The tracer used for the 6-m column experiments was NaBr with  $\text{Br}^-$  as the measured constituent. The  $\text{Br}^-$  concentration in the tracer solutions used in the experiments was 4000 mg/L  $\text{Br}^-$  (0.05 M NaBr). The analysis of the outfall water samples was accomplished with an ion-specific solid-state electrode for  $\text{Br}^-$ , Orion Model Number 9435BN, with a double junction reference electrode. While cyanide is known to interfere with ion-specific probe measurement results; the total WAD cyanide for the outfall samples measured remained below detection limit (0.01 mg/L WAD cyanide) for the duration of the experiments. Therefore, cyanide was not expected to cause significant interference. The analysis of the outfall water samples was done in the laboratory under constant temperature conditions. Ionic strength adjuster was added to the outfall samples before measuring solution  $\text{Br}^-$  concentrations as instructed by the probe manufacturer. The  $\text{Br}^-$  probe was calibrated before, during, and after the analysis of each batch of outfall water samples with standard solutions of 1, 10, 100, 1000, and 4000 mg/L  $\text{Br}^-$ .

### Column Assembly and Heap Material Placement

Spent heap material for the 6 m scale column experiments was collected from a large scale heap near Carlin, NV. This operational heap is located in the Carlin Trend, an area in northern Nevada that is presently the largest producer of gold in the USA. A backhoe was used to dig a trench approximately 3 m long and 2.5 m deep in the top of the heap. Agglomerate was collected from the bottom of this trench and placed in sealed containers until the 6-m column was assembled.

The hydraulic properties of this material were determined using data collected from a multistep outflow experiment. The hydraulic conductivity for each outflow step was determined using the inversion code MULSTPM (Eching and Hopmans, 1993a,b). The hydraulic retention function was determined using the inverse code RETC (van Genuchten et al., 1991) to be comparable to that of a very coarse sand (Table 1).

To prevent solids from passing out of the outfall tube during an experiment, five layers of fiberglass household door screen were installed into the bottom of the column. The screen has an average opening size of 1 mm. No filter pack was used on

**Table 2. Column pack data by section.**

| Section   | Bucket | Mass           | Gravimetric      | Dry bulk           |
|-----------|--------|----------------|------------------|--------------------|
|           |        |                | moisture content | density by section |
|           |        | kg             | %                | $\text{g/cm}^3$    |
| 1, Bottom | 1      | 29.50          | 5.74             | 1.40               |
|           | 2      | 27.17          | 5.25             |                    |
|           | 3      | 27.39          | 5.52             |                    |
| 2         | 4      | 27.67          | 5.16             | 1.39               |
|           | 5      | 26.79          | 5.68             |                    |
|           | 6      | 28.83          | 5.67             |                    |
| 3         | 7      | 26.92          | 5.01             | 1.39               |
|           | 8      | 28.15          | No sample taken  |                    |
|           | 9      | 22.97          |                  |                    |
| 4, Top    | 10     | 29.06          | 4.58             | 1.40               |
|           | 11     | 12.26          | 4.25             |                    |
|           |        | Total = 286.71 | Avg. = 5.19      |                    |

top of this screen. Heap agglomerate was placed into the column one section at a time. The water content analysis of samples from each of the 11 buckets used to fill the column show that the average gravimetric water content is 5.2% (Table 2). Bulk density was measured for each section during the initial installation of the agglomerate into the column (Table 2). To simulate as closely as possible the situation on the field-scale heap, no mechanical packing of the agglomerate was performed. However, after the initial wetting of the column, a significant amount of subsidence (68.6 cm) was observed after approximately one pore volume of deionized water had been run through the column. To restore the full volume, 29.28 kg of heap agglomerate was then added to the column. The dry bulk density after subsidence was 1.515  $\text{g/cm}^3$ .

### Time Domain Reflectometry Instrumentation

Time domain reflectometry was used to determine water content and bulk soil EC at eight discrete points along the length of the column and to determine breakthrough curves at eight of these length scales. The tracer experiment was initiated by injecting enough tracer into the column so that a uniformly high concentration of tracer was present. The concentration of  $\text{Br}^-$  at any time or location in the column,  $C(x,t)$ , can be expressed in normalized form as:

$$\tilde{C}(x,t) = \frac{[C(x,t) - C_0]}{[C_i - C_0]} \quad [4]$$

where  $C_i$  and  $C_0$  are the initial and pulse concentrations. The relationship between EC and concentration is:

$$\text{EC} = K_c \frac{f_t}{R_L} \quad [5]$$

where  $K_c$  is the cell constant,  $f_t$  is a temperature correction factor, and  $R_L$  is the measured probe impedance (Rhoades and van Schilfgaarde, 1976). The actual molar concentration of an ion in a solution is a function of the EC of the solution. The functional relationship between concentration and observed EC for a  $\text{Br}^-$  solution can be expressed as:

$$C[\text{Br}] = a + b(\text{EC}_{\text{br}}) \quad [6]$$

where  $C[\text{Br}]$  is the concentration of  $\text{Br}^-$ ,  $\text{EC}_{\text{br}}$  is the EC of the solution,  $a$  is the intercept, and  $b$  is the slope. This equality assumes a constant pH in the sample solution with time. We have assumed that pH remained relatively constant due to the large amount of carbonate host rock in the column acting as a buffering agent. The relationship between  $\text{Br}^-$  concentration and measured EC for a solution collected at the outfall point in the 6-m column is of the form expressed in Eq. [6]

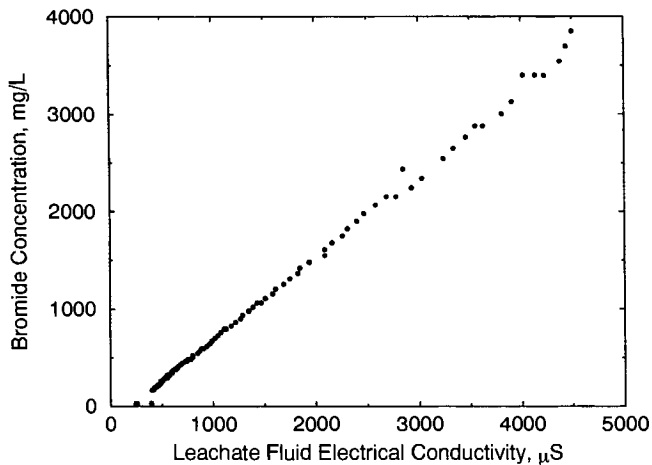


Fig. 2. Outfall sample  $\text{Br}^-$  concentration as a function of sample EC. The linear relationship between  $\text{Br}^-$  concentration and EC observed over the course of the experiment supports the use of Eq. [6]. The nonzero intercept represents the contribution to the total EC due to the dissolved ions leached from the rock during the experiment.

if it is assumed that the concentration of any other ions but the tracer ion are insignificantly small. Since the tracer solution consisted of NaBr dissolved into deionized water, this assumption is valid for this study. To demonstrate the validity of this assumption the applicability of Eq. [6] to the column experiments described in this study is illustrated in Fig. 2. Since the concentration of  $\text{Br}^-$  is directly proportional to the EC of the solution, Eq. [4] can be rewritten as:

$$\tilde{C}(x,t) = \frac{[\text{EC}(x,t) - \text{EC}_0]}{[\text{EC}_i - \text{EC}_0]} \quad [7]$$

In addition, Eq. [7] can be rewritten using Eq. [5] assuming  $K_c$  and  $f_i$  are constant as:

$$\tilde{C}(x,t) = \frac{1/R_{Lf(x,t)} - 1/R_{Lf(o)}}{1/R_{Lf(i)} - 1/R_{Lf(o)}} \quad [8]$$

if the initial concentration of tracer is uniform everywhere in the column (Mallants et al., 1994). In Eq. [8],  $R_{Lf}$  is the measured impedance after multiple reflections have occurred, and  $R_{Lf(x,t)}$  is the multiple reflection impedance at any time,  $t$ , and probe position,  $x$ .  $R_{Lf(o)}$  is the lowest measured impedance over the course of an experiment for the probe located at  $x$ , and  $R_{Lf(i)}$  is the largest measured impedance over the course of an experiment for the probe located at  $x$ . The approach shown in Eq. [8] has been used successfully to develop solute breakthrough curves across a wide range of solution salinity (Kachanoski et al., 1992; Mallants et al., 1994).

The equations expressed above are for the special case where the initial concentrations of a solute are at a maximum throughout the column. In this study, the initial concentration of  $\text{Br}^-$  in the 6-m column was 4000 mg/L throughout the column. The column was then rinsed with deionized water with a  $\text{Br}^-$  concentration of 0 mg/L. If a pulse experiment were to be conducted and EC measured with TDR, then the cell constants and temperature correction factors would have to be determined for each probe placed into the 6-m column. By confining the tracer experiments to the special case where the initial concentration of solute is at a maximum everywhere in the column, the problems associated with calibrating the TDR wave guides are effectively eliminated through the mathematical cancellation of the temperature and the cell constants.

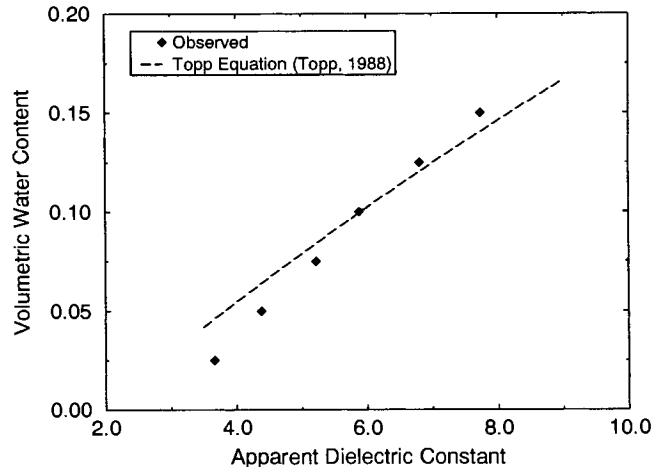


Fig. 3. Time domain reflectometry probe response as a function of water content calibration to the heap material used in the 6-m scale column experiments (Topp et al., 1988).

### Time Domain Reflectometry Volumetric Water Content Calibration

Volumetric water content can be determined from TDR measurements using an empirical expression, the Topp equation (Topp et al., 1980). However, the soils used to develop this expression were all relatively uniform, fine grained agricultural soils. For this study, the probe was calibrated from known volumetric water contents in the heap material and a modified Topp equation was developed for it.

The calibration was conducted using a 35 cm long section of the tubing that comprised the 6-m column. The calibration cell was packed with a 15-kg charge of oven-dried heap material to a dry bulk density of 1.58 g/cm<sup>3</sup> and a TDR probe installed. This compares to a calculated dry bulk density of the 6-m column of 1.52 g/cm<sup>3</sup>. A TDR trace was then taken and the cell emptied into three containers. Water was added to each container to raise the volumetric water content to 2.5%. The cell was repacked with the TDR probe, and a second TDR trace taken. This procedure was repeated for 5.0, 7.5, 10.0, 12.5, and 15% volumetric water contents. The calibration curve shown in Fig. 3 is the best-fit linear regression line, with a correlation coefficient of 0.9984. It is described by the relation

$$\theta_v = -0.0854 + 0.03079(K_a) \quad [9]$$

where  $K_a$  is the apparent dielectric constant.

## RESULTS

### Analysis of U.S. Bureau of Mines Experimental Data

The U.S. Bureau of Mines Reno Research Center conducted column studies of heap material collected from four mine sites in Nevada (Comba et al., 1992; Dix et al., 1992). This work consisted of performing six conservative tracer flow experiments in 1.2 and 5.4 m tall by 14 cm diameter columns. The breakthrough data were analyzed by the authors of this paper using both an ADE and a dual-porosity model. An example of the fitting performance of these models to one of the USBM tests is illustrated in Fig. 4. In general, the dual-porosity model provided a significantly improved fit to the observed breakthrough curve as a whole, and to the tail

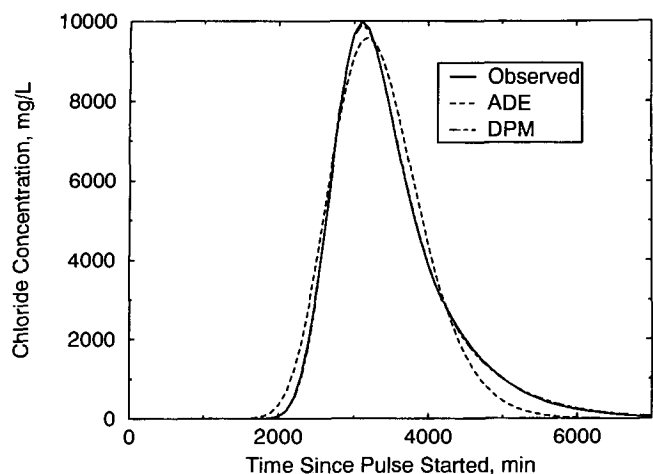


Fig. 4. A comparison of the ADE and dual-porosity model inversion fit results to a sample USBM column tracer experiment dataset. The tracer is NaCl at a concentration of 260 000 mg/L and an initial pulse width of 55 min. An inline EC probe was used to track the breakthrough profile at the bottom of the 1.2 m tall column. The dual-porosity model provides a visually improved fit to the observed breakthrough curve as compared with the ADE inversion result, particularly at long rinse times.

part of the breakthrough curve in particular. A plot of  $R^2$  values for the ADE and dual-porosity models is shown in Fig. 5, and illustrates that the  $R^2$  values for the dual-porosity model are higher in all cases than the ADE model.

### Solute Transport Process Analysis, 6-Meter Column Experiment, Carlin Heap Material

A total of five tracer experiments were completed using NaBr as a tracer in the 6-m column. Due to an experimental design flaw that was not detected until the start of the last experiment, only TR-05 was successful in developing breakthrough curves from TDR EC data and this is the only dataset reported. The breakthrough curve developed from the  $\text{Br}^-$  analysis of the outfall water for this experiment is given in Fig. 6 along with the ADE and dual-porosity model fitting results and the model fitting parameters are given in Table 3. These

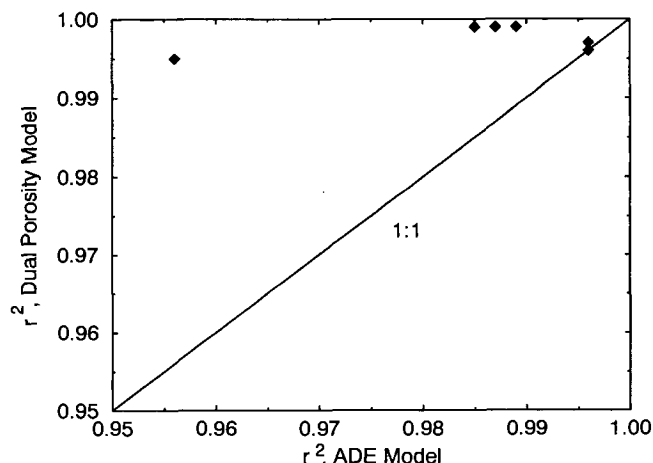


Fig. 5. A comparison of model  $R^2$  for the USBM column tracer experiments, which shows that the dual-porosity model is an improvement over the ADE model inversion results.

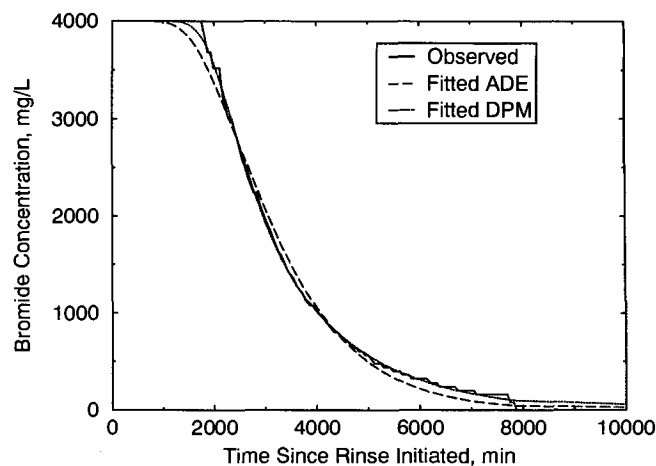


Fig. 6. A comparison of the ADE and dual-porosity model inversion fit results for the 6-m scale column tracer experiment TR-05 outfall (scale length 595 cm) data. The dual-porosity model provides a visually improved fit to the observed breakthrough curve as compared with the ADE inversion result, particularly at long rinse times.

results, and those from the other four tracer experiments are consistent with the inverse model results from the USBM datasets. The dual-porosity model provides a statistically improved fit over the ADE model and demonstrates a significant improvement in the estimation of concentration of solute at long rinse times.

### TR-05 Time Domain Reflectometry Data and Model Inversion Results

The TDR data for experiment TR-05 were analyzed using the methods given in Zeglin et al. (1989) and Mallants et al. (1994), as described previously. Figure 7 is a concatenation of all of the TDR-derived breakthrough curves for TR-05. The TDR-derived breakthrough curves were analyzed using CXTFIT (Parker and van Genuchten, 1984) with both the simple ADE model and the dual-porosity model. The outfall  $\text{Br}^-$  concentration data were modeled as flux-averaged concentration while the TDR-derived solute concentration data were modeled as resident concentration. The inversion results for the ADE model and the dual-porosity model are given in Table 4. The ADE and the dual-porosity model solutions for Probe 4, located in the middle of the column, are given in Fig. 8, and a plot of  $R^2$  for the ADE and dual-porosity models is shown in Fig. 9. Based on a simple statistical parameter,  $R^2$ , the dual-porosity model demonstrates only a slight improvement in matching the observed breakthrough data

Table 3. Summary of model fitting parameters for outfall data.

| Parameter                                              | Value                     |                          |
|--------------------------------------------------------|---------------------------|--------------------------|
|                                                        | ADE Model                 | MIM Model                |
| Velocity, $V$ , cm/min                                 | $0.18 \pm 5.26\text{E-}3$ | $0.17 \pm 6.8\text{E-}4$ |
| Dispersion coefficient, $D$ , $\text{cm}^2/\text{min}$ | $9.93 \pm 1.95$           | $2.92 \pm 3.60$          |
| Dispersionity, $\alpha$ , cm                           | $55.89 \pm 5.35$          | $16.88 \pm 18.74$        |
| Mobile mass fraction, $\beta$                          | —                         | $0.75 \pm 0.16$          |
| Mass transfer coefficient, $\omega$                    | —                         | $0.73 \pm 0.91$          |
| Correlation coefficient, $R^2$                         | 0.95                      | 0.96                     |

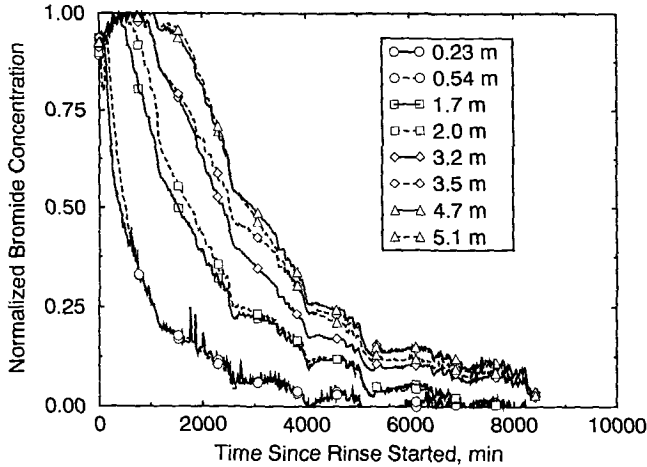


Fig. 7. A concatenation of TDR-derived breakthrough curves for the 6-m scale TR-05 tracer experiment. Included with the TDR-derived breakthrough curves is the breakthrough curve resulting from the inversion of the Br<sup>-</sup> concentration data collected at the column outfall at a scale length of 5.94 m.

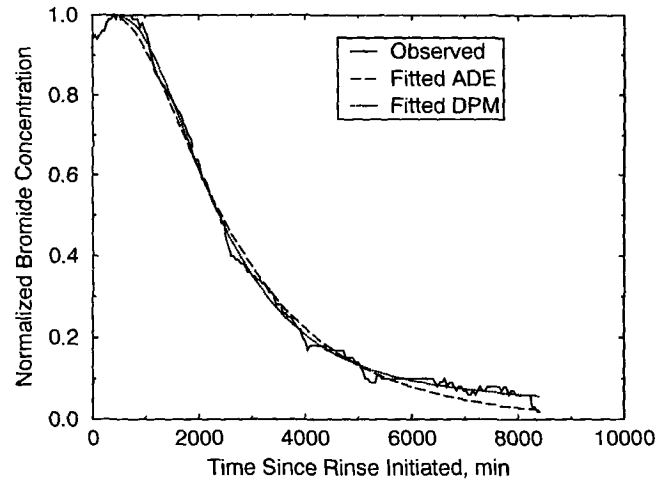


Fig. 8. A comparison of the ADE and dual-positivity model inversion fit results to a breakthrough curve calculated from TDR EC data at the 3.2 m length scale for the 6-m scale TR-05 tracer experiment.

for the eight TDR-derived breakthrough curves over the simple ADE model (Fig. 9). However, the dual-positivity model provides, visually, a more representative estimation of solute concentration at long rinse times than the ADE model. This result is economically significant in terms of heap rinse times.

**Mass-Balance Results for Tracer Experiment TR-05**

To confirm that the TDR-derived breakthrough curves are consistent with the outfall breakthrough curve for TR-05, a mass balance calculation was performed with both the outfall and the TDR-derived breakthrough curves. The results of this calculation indicate that compared with the outfall data the TDR overestimates the amount of mass remaining in the column (Fig. 10). This calculation incorporated the entire volume of the column, including the uncharacterized saturated zone at the bottom of the column. To eliminate the unknown solute mass held in the saturated zone, a second calculation of mass balance was made at 520 cm. Time domain reflectometry Probe 1 is located at 510 cm, and 520 cm was selected as a convenient discretization location that probably is above the saturated zone. The results of the dual-positivity inversion of the outfall data

at 595 cm were used to simulate a breakthrough curve at 520 cm. This simulated curve was then used to generate a mass remaining curve to compare with the TDR breakthrough mass balance curve (Fig. 11). Though the apparent error between the outfall and the TDR-derived results is still large, there is a significant improvement over the mass balance calculation done at 595 cm. The improvement is due to excluding the unknown amount of solute mass in the saturated zone below 520 cm. Moreover, CXTFIT assumes that there is a uniform water content throughout the column; but the TDR results show that there is some variability in water content. This results in an immediate mass accounting discrepancy between the TDR-derived result and the CXTFIT inversion of the outfall Br<sup>-</sup> concentrations.

**Discussion of Derived Solute Transport Parameters**

The breakthrough curves derived from the TDR EC data were used to develop the flow and transport parameters using both the ADE and dual-positivity models. The solute velocities for experiment TR-05 are plotted for comparison on Fig. 12 from the following sources: the TDR-derived breakthrough curve inversions for both the ADE and dual-positivity models, TDR-derived volumetric water content, and the CXTFIT inversion

Table 4. Time domain reflectometry probe-derived breakthrough curve model fit results.

| Parameter               | Probe no.: length scale, m |             |             |              |              |              |             |             |
|-------------------------|----------------------------|-------------|-------------|--------------|--------------|--------------|-------------|-------------|
|                         | 8:0.23                     | 7:0.54      | 6:1.7       | 5:2.0        | 4:3.2        | 3:3.5        | 2:4.7       | 1:5.1       |
| <b>ADE Model</b>        |                            |             |             |              |              |              |             |             |
| V, cm/min               | 0.09 ± 0.02                | 0.14 ± 0.02 | 0.14 ± 0.01 | 0.15 ± 0.01  | 0.14 ± 0.01  | 0.14 ± 0.01  | 0.18 ± 0.01 | 0.19 ± 0.01 |
| D, cm <sup>2</sup> /min | 7.37 ± 3.62                | 7.37 ± 3.62 | 6.27 ± 1.45 | 7.70 ± 1.81  | 11.90 ± 2.16 | 16.55 ± 2.91 | 7.18 ± 1.38 | 7.44 ± 1.39 |
| α, cm                   | 42.5 ± 20                  | 53.8 ± 24   | 46.4 ± 3.6  | 51.4 ± 5.4   | 86.0 ± 8.5   | 124.0 ± 16   | 40.8 ± 2.8  | 39.5 ± 2.6  |
| R <sup>2</sup>          | 0.84                       | 0.87        | 0.95        | 0.94         | 0.94         | 0.95         | 0.96        | 0.97        |
| <b>MIM Model</b>        |                            |             |             |              |              |              |             |             |
| V, cm/min               | 0.05 ± 0.04                | 0.10 ± 0.04 | 0.09 ± 0.02 | 0.09 ± 180   | 0.11 ± 0.07  | 0.11 ± 0.06  | 0.13 ± 0.01 | 0.15 ± 0.01 |
| D, cm <sup>2</sup> /min | 1.18 ± 2.86                | 2.85 ± 4.89 | 2.29 ± 4.07 | 7.65 ± 1.5E5 | 6.20 ± 2.97  | 9.68 ± 4.07  | 5.79 ± 2.90 | 5.38 ± 2.94 |
| α, cm                   | 21.8 ± 39                  | 29.6 ± 62   | 23.4 ± 44   | 78.0 ± 2E12  | 56.5 ± 20    | 85.2 ± 36    | 44.6 ± 17   | 36.3 ± 14.6 |
| β                       | 0.45 ± 0.41                | 0.59 ± 0.34 | 0.52 ± 0.30 | 0.73 ± 1E4   | 0.77 ± 0.48  | 0.79 ± 0.33  | 0.74 ± 0.06 | 0.77 ± 0.07 |
| ω                       | 0.39 ± 0.50                | 0.26 ± 0.41 | 0.85 ± 0.75 | 6E.9 ± 0.06  | 0.08 ± 0.19  | 0.08 ± 0.33  | 0.23 ± 0.29 | 0.27 ± 0.31 |
| R <sup>2</sup>          | 0.86                       | 0.88        | 0.94        | 0.94         | 0.95         | 0.95         | 0.96        | 0.96        |

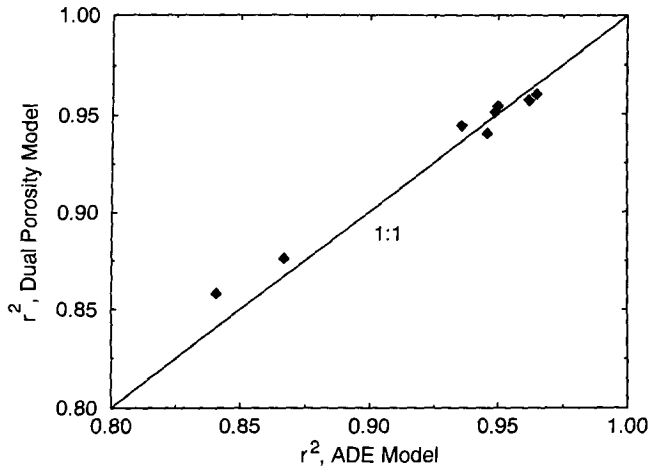


Fig. 9. A comparison of the ADE and dual-porosity model model  $r^2$  for the TDR-derived breakthrough curve dataset for all length scales in the 6-m scale column tracer experiment. The dual-porosity model shows a marginal improvement over the ADE model inversion results.

of the outfall  $\text{Br}^-$  concentrations. Inversion of the TDR-derived breakthrough curves indicates that solute velocity appears to increase with scale length. However, the solute velocity that is calculated from the applied flux and observed volumetric water contents indicate a decreasing velocity with scale length, consistent with the water content increase with depth. Theoretically, the TDR-derived solute velocities and those calculated using volumetric water content should be very similar, and should certainly follow the same trend with scale length.

The inversion code used to calculate solute velocity from the TDR EC data, CXTFIT, assumes that the column is under uniform conditions. However, the column water content, as measured by TDR, increases with depth. This is consistent with the parameters of the experiment, as the outfall of the column was not placed under matric tension. Therefore, for fluid to exit the

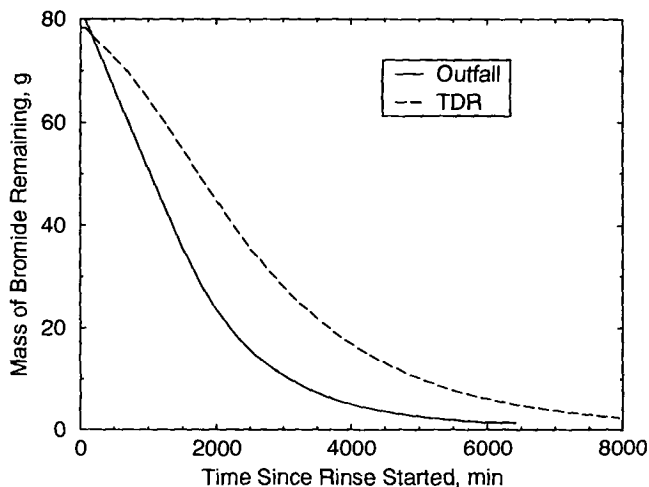


Fig. 10. A comparison of calculations of mass remaining in the 6-m column made with outfall data and TDR EC data for experiment TR-05. Both calculations are made at the outfall point in the column. The difference between the two results is due to the amount of unknown solute mass held in the saturated zone at the bottom of the column.

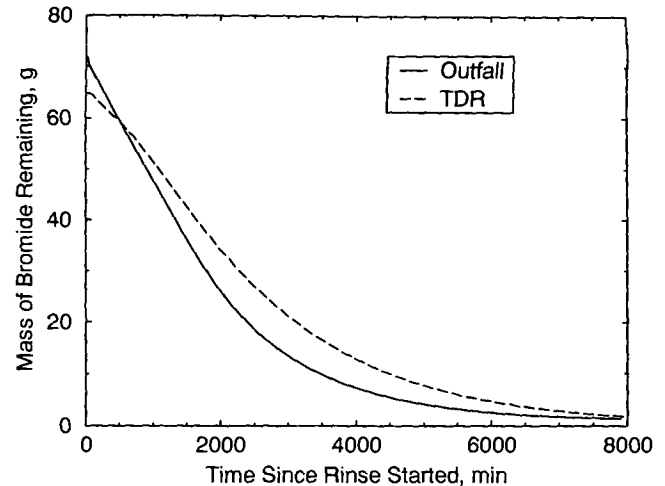


Fig. 11. A comparison of calculations of mass remaining in the 6-m column made with outfall data and TDR EC data for experiment TR-05. The mass remaining calculation is rescaled to a column length of 520 cm to negate the effects of the saturated zone at the bottom of the column. The rescaling effort results indicate a significant improvement in mass balance agreement between the outfall and TDR-derived mass remaining curves.

column, a saturated zone had to exist near the bottom of the column.

The velocity relationships shown in Fig. 12 can be addressed through a discussion of the physics of the TDR measurement. The solute velocity trends calculated from the inversion of the TDR EC data near the top of the column are much lower than what would be expected from velocities calculated from water content information (Fig. 12). The TDR method provides a volume average from the porous media surrounding the TDR probe, which includes the mobile and immobile water solute mass contributions. The 6-m tracer experiment was conducted with an initially high solute concentration and the rinse solution was deionized water. Ow-

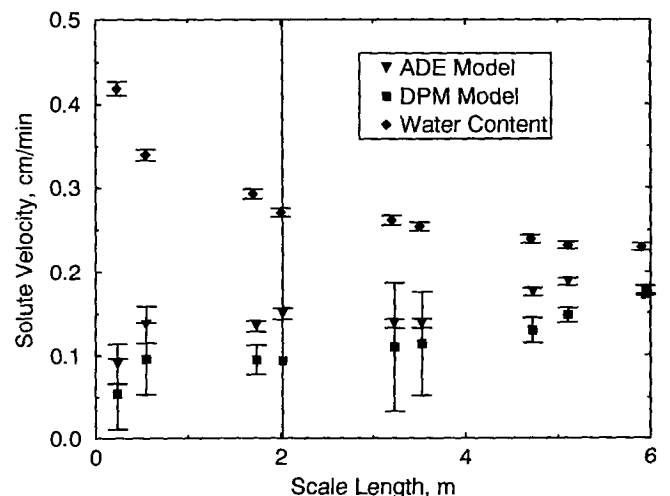


Fig. 12. A comparison between solute velocity calculated from TDR water content and the inversion of the solute breakthrough curves generated from TDR EC data. Both the ADE and dual-porosity model inversion results are shown. The differences between the water content derived velocity and the velocity determined from the inversion of TDR EC data is due to the volume averaging characteristics of the TDR measurement of soil properties.

ing to TDR's averaging of the mobile and immobile water contributions, at early rinse time the TDR EC data will not be sensitive to changes in the mobile water solute concentration because most of the solute mass is still held in the immobile pore spaces. Therefore, the TDR will measure an average EC that will remain high until enough solute mass has moved from the immobile pore spaces and is flushed out of the TDR sample volume. The time required to affect this change in volume averaged EC is much longer than that required to alter the EC in the mobile pore spaces. Thus, if the conductivity measured with TDR is used to calculate a solute velocity, the result will resemble a retarded velocity profile. The volume averaging aspect of the TDR measurement does not allow a direct comparison of the TDR-derived solute velocities with either the resident or flux-averaged velocity results.

The trend of increasing solute velocity with depth demonstrated in the TDR EC data is consistent with the expected effects of lateral dispersion. The presence of lateral dispersion, or spreading, of the solute breakthrough front would allow solute transfer from the immobile pore spaces before the average velocity front arrives, resulting in an apparent increase in solute velocity with an increase in scale length.

#### **Dispersivity, Mobile Mass Fraction, Mass Transfer Coefficient**

The solute transport parameters for both the ADE and dual-porosity models do not demonstrate scale-dependent behavior (Table 4). The value of dispersivity remains nearly uniform at a value of approximately 1.0 m with an increase in scale length when the width of the 95% confidence interval is taken into consideration. In addition, the mobile mass fraction ( $\beta$ ) is nearly constant throughout the length of the column at about 75%. Therefore, 25% of the material in the column is behaving as though contained in immobile pore spaces. The transfer of solute between the mobile and immobile pore spaces is controlled by the mass transfer coefficient, which is also nearly constant with depth. The representative value of approximately 0.40 can be combined with the solute velocity and the column length to provide an estimate of the time scale of mass transfer between the mobile and immobile fractions (20 d).

The results of the development and subsequent inversion of the TDR-derived breakthrough curves have identified a flow and transport process that was previously suspected, but not as yet identified: the presence of a variable velocity field. The dual-porosity model is an approximation of a velocity distribution. It effectively provides two velocities with the additional description of the percentage of porous media assigned to each velocity. However, the true velocity distribution is certainly not simply two discrete velocities, but an entire distribution, or range of velocities. The true significance of the dual-porosity model in this instance is that it represents a closer approximation to a multipoint velocity distribution than does the simple advection-dispersion equation.

With this enlightened understanding of the flow and

transport processes in heap material, and with the flow and transport parameters determined for the study material, it is now possible to construct a model of a field-scale heap, and to estimate the rinse performance of a nonreacting, nonsorbing solute from the heap.

#### **FORWARD MODELING OF FIELD-SCALE HEAP AND DISCUSSION**

The experiments and results described so far have been limited to the laboratory, or near-field-scale. This information is important because it identifies the main transport processes in a heap and the hydraulic and solute transport characteristics for the material studied. These can then be used to estimate the rinse behavior of a field scale heap.

The analysis of the breakthrough curve data from both the USBM datasets and the tracer experiments completed with the 6-m column on the Carlin material indicate that the dual-porosity model is a more appropriate representation of the true hydraulic and solute transport processes in a heap. The dual-porosity model provided significantly improved breakthrough curve fits as compared with the ADE model, for the range of materials studied by the USBM. In addition, the dual-porosity model was more successful in fitting a breakthrough curve to the 6-m column outfall and TDR-derived data. The dual-porosity model was therefore used to simulate cyanide transport at the field-scale.

To develop an improved understanding of the field-scale heap during cyanide rinsing, the hydraulic and solute transport parameters developed through experimentation were applied in a forward model of the full size heap. This predictive model can then be used to develop breakthrough curves at length or time scales set by the user. The results of this calculation will provide information relating the scale of the heap to rinse times and efficiencies. Thus, an estimate of field-scale heap rinse performance may be possible with hydraulic and solute transport information from laboratory or near field-scale column experiments.

#### **Forward Model of a Hypothetical Heap**

The numerical code used for the forward calculations was CXTFIT. The model simulates a one-dimensional vertical column 30.48 m tall of heap material identical to that found at the Carlin site. Additionally, the material is assumed to be homogeneous and isotropic with a time-invariant velocity field and a dispersivity of 1.0 m. The assumption of a uniform velocity field is not precisely correct due to the heterogeneity of the heap material and the presence of a saturated zone near the heap liner. However, this assumption is chosen for simplicity at this point. The top and bottom of the modeled column are subjected to a specified flux. For the purposes of this simple model, it was assumed that no other sources/sinks of water exist at the top of the column other than the applied rinse water. The initial concentration conditions were that 20 mg/L of a nonreactive, nonsorbing, conservative solute present throughout the column and that the rinse water had a concentration of 0 mg/L

of solute. The concentration conditions are representative of cyanide concentrations at the onset of heap rinsing. The assumption of solute conservation is not, however, directly applicable to cyanide, which is subject to degradation, sorption, and other nonconservative attenuation processes. However, the simulation results presented represent a conservative estimate of cyanide transport through a heap during rinsing. Most of the minerals that react with cyanide can be assumed to have done so during the production phase of the heap. In addition, since the cyanide ion is negatively charged the potential for sorption onto clays is low. Therefore, though not correct in the strictest geochemical sense, the use of a conservative tracer as an analog for cyanide transport during heap rinsing remains as a useful approximation for the purposes of this study.

The values of the flow and transport parameters used in the forward model are representative of those derived from the inversion of the 6-m column experiments with the Carlin heap material. Since CXTFIT does not have the capability of including a time varying application rate, a uniform, constant pulse of 0 mg/L solute water was admitted to the top of the simulated heap. In practice, the application of fluid onto the heap is pulsed due to the volume handling limitations of the leachate water processing plant.

Aside from the input flux pulse width, there are four parameters that are used in the dual-porosity model: water velocity, dispersivity, mobile mass fraction coefficient, and the mass transfer coefficient. The solute velocity is set by the application rate, assuming that a unit-hydraulic gradient exists in the heap. The dispersivity is a function of the solute velocity and the dispersion coefficient, and is a property of the porous media. The mobile mass fraction coefficient and the mass transfer coefficient are both specific to the dual-porosity model, and describe the interaction between the two idealized porosities in the porous medium.

Both the mobile mass fraction and the mass transfer coefficient are likely to be functions of the applied flux. The mobile mass fraction, which is the ratio of the mobile water content to the total water content, should rise with an increase in applied flux. The increase in total water content with an increase in applied flux is determined from the  $K(\theta)$  relationship for the material in question. Because the immobile water is held in dead end pore spaces, an increase in applied flux should not significantly increase the immobile water content. Therefore, an increase in applied flux will result in an increase in the mobile mass fraction.

The mass transfer coefficient,  $\omega$ , is a function of the first-order rate coefficient,  $\alpha^*$  ( $1/T$ ),

$$\omega = \frac{\alpha^* L}{q} \quad [10]$$

where  $L(L)$  is the column length and  $q$  is the solute velocity ( $L/T$ ). The mobile mass fraction and the first-order rate constant,  $\alpha^*$ , are assumed to be independent of the applied flux and the volumetric water content. The value of  $\alpha^*$  used in the forward simulations,  $\alpha^* =$

**Table 5. Calculated values of  $\omega$  and  $\theta$  for a range of applied fluxes.**

| Applied flux | $\omega$ | $\theta$ | $V$    |
|--------------|----------|----------|--------|
| cm/min       |          | %        | cm/min |
| 0.0068       | 9.67     | 7.08     | 0.096  |
| 0.0136       | 4.84     | 7.24     | 0.188  |
| 0.0204       | 3.22     | 8.36     | 0.244  |
| 0.0245       | 2.68     | 10.27    | 0.239  |
| 0.0306       | 2.15     | 15.66    | 0.195  |

$2.16E-5 \text{ min}^{-1}$ , was determined from the inversion of the tracer breakthrough data from the 6-m column experiments.

Of the four parameters used in the dual-porosity model, the parameter that is most easily varied is the solute velocity, since the heap operator can manipulate the solute velocity by adjusting the rinse fluid application rate. The dispersivity cannot be altered without large scale mechanical modification to the heap material. Both the mobile mass fraction and the mass transfer coefficient are functions of the volumetric water content, and are not adjustable independently of the applied flux rate. Therefore, from a cyanide rinsing standpoint, the most important operational parameter for the forward model results presented is the solute velocity.

## FORWARD MODELING RESULTS

### Determination of the Mass Transfer Coefficient for the 30.5 M Scale

The forward simulations of the Carlin heap were conducted with a range of applied fluxes. Because  $\omega$  is a function of the applied flux, the value of  $\omega$  for each applied rinse rate value is unique. In addition, due to the coupled relationship between the  $K(\theta)$  curve and solute velocity, a unique water content exists for each value of applied flux. The values of  $\omega$  calculated for this series of simulations and the volumetric water contents determined from the  $K(\theta)$  relationship are given in Table 5.

### Rinse Fluid Application Rate (Solute Velocity)

A commonly used application rate is 0.1758 L/min per  $\text{m}^2$ , which corresponds to a water flux of 0.0204 cm/min. The application rates modeled were 0.0598, 0.1160, 0.1758, 0.2110, and 0.2637 L/min per  $\text{m}^2$ . The values of dispersivity (1.0 m) and the mobile mass fraction (0.75) parameters corresponded to values observed from the 6-m column experiments previously discussed. The values of the mass transfer coefficient were calculated for the applied rinse application rates modeled, and are given in Table 5. The values of the solute velocity parameter,  $V$ , used in CXTFIT, were calculated using the hydraulic retention and  $K(\theta)$  relationships for the Carlin heap material. Solute velocity is defined as:

$$V = \frac{q}{\theta_t} \quad [11]$$

where  $q$  is the applied flux, and  $\theta_t$  is the total volumetric water content determined from the  $K(\theta)$  curve. By assuming that a unit hydraulic gradient exists throughout

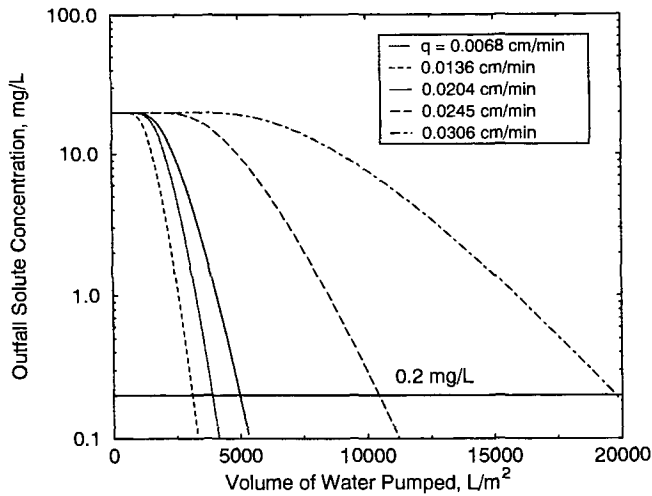


Fig. 13. The results of modeling the rinse behavior of a nonreacting, nonsorbing solute from a 30.5-m scale hypothetical heap. The simulated heap is 30.5 m tall with a dispersivity of 1.0 m and a mobile mass fraction ( $\beta$ ) of 0.75. The rinse time required to lower the solute concentration in the outfall fluid one order of magnitude is a nonlinear function of rinse application rate.

the heap,  $q = K$ , and  $\theta_i$  is then easily determined. The value of  $\theta_i$  for each applied flux value used in the model is also given in Table 5.

#### Mass Transfer Coefficient ( $\omega$ )

The results shown in Fig. 13 show the relationship between rinse water volume pumped and the solute concentration at the outfall for the modeled rinse application rates. These results are restated in Fig. 14 but with rinse volume plotted against the mass of cyanide remaining in the heap. In Fig. 13, there is a nonlinear relationship between rinse rate and the rinse volume required to reach an outfall cyanide concentration of 0.20 mg/L. A rinse application rate of 0.0136 cm/min results in a reduced volume of water required to rinse the cyanide from the heap as compared with either the next smallest rinse rate or any of the larger rinse rates. This observation is clearly evident in Fig. 14, which shows that the rinse rate of 0.1160 L/min per  $m^2$  requires substantially less water to drive the outfall cyanide concentration to 0.20 mg/L than any of the remaining four rinse application rates.

The first three flux rates modeled, 0.0068 to 0.0204 cm/min, all have nearly the same volumetric water contents; however, their mass transfer coefficients are very different. The apparent transposition of the calculated breakthrough profiles for the 0.0136 and 0.0068 cm/min applications is because the latter is associated with an  $\omega$  nearly twice that for the former. The flux of solute between the mobile and immobile phases in the model depends on  $\alpha^*$  (a constant incorporated into  $\omega$ ) and the concentration gradient between the mobile and immobile porosities. The large value of  $\omega$  for the 0.0068 cm/min flux represents an exchange rate between the mobile and immobile porosities in the model that is twice that for the 0.0136 cm/min flux. Because of the high exchange rate between the two porosities for the 0.0068 cm/min simulation, the concentration gradient is small-

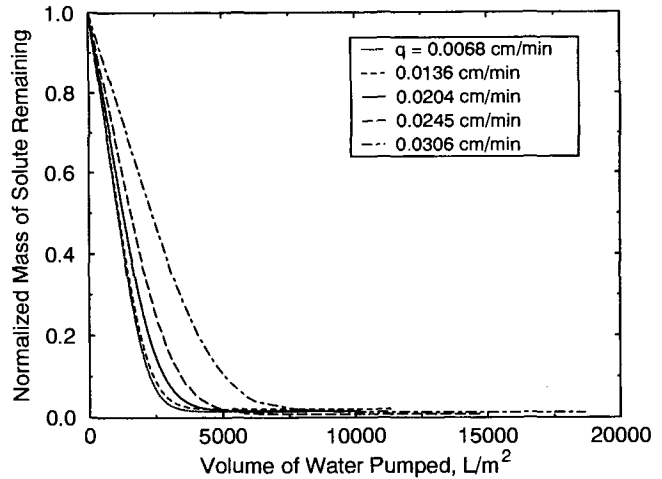


Fig. 14. The results of modeling the rinse behavior of a nonreacting, nonsorbing solute from a 30.5-m scale hypothetical heap. The simulated heap is 30.5 m tall with a dispersivity of 1.0 m and a mobile mass fraction ( $\beta$ ) of 0.75. The rinse time required to lower the solute concentration in the hypothetical heap one order of magnitude is a nonlinear function of rinse application rate.

er. The 0.0136 cm/min flux maintains a higher concentration gradient between the immobile and mobile porosities, and the cyanide concentration in the outfall reaches the target concentration of 0.20 mg/L ahead of the 0.0068 cm/min flux. This effect is nonlinear, and it is possible that a lower flux rate than 0.0136 cm/min exists that would result in a smaller rinse volume of requirement than for the 0.0136 cm/min result shown here.

The remaining two flux values modeled, 0.0245 and 0.0306 cm/min, result in very large volumes of water required to remove cyanide from the outfall, or mobile water. This result is due in part to the low values of  $\omega$  for these flux values, but is most strongly a function of the large volumetric water contents for these flux values. The large volumetric water contents result in a significant increase in the amount of cyanide mass initially in the column. Therefore, the long rinse times required for the two highest flux rates are due, in part, to the fact that a much larger mass of cyanide must be removed than for the lower flux values modeled. The dependence of initial cyanide mass on water content is a modeling artifact of the forward simulations. The mass of cyanide in the heap during production is dependent on the leach solution flux. However, once production has ceased, the field-scale heap is at some constant initial mass of cyanide, regardless of the applied rinse fluid flux.

#### Applications to Understanding Field-Scale Heap Rinsing Behavior

During a pulsed rinse application, the outfall cyanide concentration will cycle between the rinse water concentration and the equilibrium concentration between the mobile and immobile phase. For example, if the rinse water application at the surface of the heap is ceased, the cyanide in the immobile phase will continue to diffuse into the mobile phase. Thus, with time, the mobile and immobile cyanide concentrations will equilibrate and once the rinse water application is reinstated, the

outfall concentration will elevate to concentrations nearly equal to those concentrations observed at the beginning of the previous rinse cycle. This phenomenon has been observed during the rinsing of field-scale heaps. The rate at which the mass diffuses between the mobile and immobile phases of the porous media is described by the mass transfer coefficient.

For smaller values of  $\omega$ , the rate of mass transfer is relatively slow, and the initial breakthrough occurs earlier since the mass in the mobile phase is removed quickly, and not replaced by mass from the immobile phase at a rate high enough to maintain the concentration of cyanide in the mobile phase. Thus, the shape of the breakthrough curve is dependent in part on the concentration gradient between the two phases. Because the mass held in the immobile phase diffuses into the mobile phase during rinsing, for smaller values of  $\omega$ , the breakthrough curves will appear to have an increasingly longer tail as compared to larger values of  $\omega$ .

The conclusion regarding optimal applied rinse flux that is based solely on Fig. 13 is that a flux of 0.0136 cm/min results in satisfying the cyanide concentration requirement with the least amount of applied rinse water. However, the results presented in Fig. 14 indicate that to drive the cyanide out of the heap in the most economical manner, a rinse flux of 0.0245 cm/min should be used. This rinse flux results in the lowest mass of cyanide remaining in the heap, with the least amount of pumped water applied to the heap. Though this flux rate requires much larger volumes of applied rinse water to drive the outfall cyanide concentration below the 0.20 mg/L target value than the 0.0136 cm/min flux, the fact that the 0.0245 cm/min flux removes the most cyanide from the heap with the least amount of applied rinse volume governs the selection of the optimal applied rinse flux. It is important to note that while the 0.0068 cm/min flux rate appears to lower the amount of mass remaining in the heap more rapidly than any other flux rate, the volume of rinse water required to lower the heap cyanide concentration two orders of magnitude (20–0.20 mg/L) is off the end of the scale shown in Fig. 14. In a pulsed rinse application, the mass remaining in the heap with the use of the 0.0068 cm/min flux would likely drive the outfall concentration above the 0.20 mg/L cyanide concentration target, and an additional volume of rinse water would then have to be applied. Thus, the outfall concentration requirement is directly coupled to the mass of cyanide in the heap, and without the removal of cyanide from the heap, the outfall concentration target of 0.20 mg/L cannot be reached.

## SUMMARY AND CONCLUSIONS

By utilizing TDR to measure bulk EC, and to then use the bulk EC to develop breakthrough curves at several length scales, it is possible to gain new insight into the mechanisms of hydraulic and solute transport that is not possible by studying the outfall results alone. With the outfall results, the conclusion can be made that solute mass is held in both advective and nonadvective fractions within the porous media. The results of the

TDR-derived breakthrough curve analysis for experiment TR-05 suggest that rather than a true dual-porosity process, a highly heterogeneous velocity flow field exists, which can be approximated by the dual-porosity model.

The new conceptual model also explains the phenomenon of cyanide concentrations rising after an apparently acceptable value has been reached during rinsing. This results from the presence of an immobile mass fraction with a cyanide mass whose transport is diffusion limited. To illustrate, for large immobile mass fractions, the mass of cyanide remaining in the heap after extensive rinsing can be significant. The mass remaining in the heap diffuses into the mobile pore spaces at a rate limited by the mass transfer coefficient. If, after an extensive rinsing period, the rinse water application is then stopped, the cyanide mass held in the immobile regions in the heap will diffuse into the mobile areas as defined by the mass transfer coefficient. The concentration of cyanide in the mobile regions in the heap will eventually equilibrate with the immobile cyanide concentration, thus elevating the concentration of cyanide in the mobile regions. Upon reinstatement of rinsing, the outfall concentration of cyanide will rise as the mobile fraction is removed.

The rinsing of cyanide from a spent heap is a function of the four parameters used in the dual-porosity model. However, only one of these parameters, rinse fluid application rate, is assumed to be controllable. The mobile mass fraction ( $\beta$ ) and the first-order rate coefficient ( $\alpha^*$ ) contained within the definition of the mass transfer coefficient ( $\omega$ ) are functions of the applied flux and, subsequently, the water content. However, at present, there are no data available regarding the functional relationships between these parameters and water content. The results of the modeling previously described indicate that it is possible to optimize the rinse flow rate to the amount of fluid required to remove the cyanide from the heap and from the leachate (outfall) water. The modeling results also indicate that a larger applied flux than the 0.0204 cm/min commonly used would result in a smaller net volume of water required to remove the cyanide from both the heap and the outfall (leachate) water. However, the relationship between application rate and required rinse volume is nonlinear due to the dependence of the solute velocity on total volumetric water content, and the nonlinear relationship between applied flux and the mass transfer coefficient.

This work describes an effort to develop an understanding of the hydraulic and solutransport characteristics of precious metals recovery heap operations. An analysis of tracer tests conducted on a wide range of heap materials has provided both new insight into the flow processes in a heap and, at the same time, has provided support for a dual-porosity model that provides improved estimates of the hydraulic and solute transport behavior of a heap. The use of cyanide as a leaching agent is an economic and mining engineering success. However, there is an environmental cost associated with the use of cyanide due to the extreme toxicity of it to animals and people. Therefore, developing an

understanding of the flow and transport behavior of cyanide in mine heap structures is critical to designing heap rinse strategies. The effort described here takes a step toward this understanding through a description of the physical transport processes in a heap. In addition to being able to evaluate heap rinsing strategies, the model may also be of value in predicting heap leach efficiency before construction. With the incorporation of cyanide chemical pathways and kinetics, it may be possible to predict, based on the physical flow and transport model presented here, precious metals recovery efficiencies. The same flow processes occur for both rinsing and leaching of heap-leach piles; thus, the model is applicable to an estimation of heap-leach production behavior.

### ACKNOWLEDGMENTS

This work would not have been possible without the help of the Barrick Goldstrike Mines. A special thanks to Paul Comba and Russ Dix of the former USBM for their contributions in the initial formulation of the project and subsequent experiments. Funding for this work was provided by NCERQA USEPA grant no. R825289-01-0 and by the U.S. Bureau of Mines Generic Mineral Technology Center, Minerals Industry Waste Treatment and Recovery grant no. G113-5232.

### REFERENCES

- Cathles, L.M., and L.E. Murr. 1980. Evaluation of an experiment involving large column leaching of low grade copper sulfide waste: A critical test of a model of the waste leaching process. p. 29-48. *In* W.J. Schlitt (ed.) *Leaching and recovering copper from As-mined materials*. SME of AIME. Am. Inst. of Mining, Metallurgical and Petroleum Eng., New York.
- Coats, K.H., and B.D. Smith. 1964. Dead-end pore volume and dispersion in porous media. *Soc. Pet. Eng. J.* 4:73-84.
- Comba, P.G., R.B. Dix, and S.L. McGill. 1992. A field study to assess natural degradation of cyanide species in an inactive leached ore heap. p. 535-543. *In* Proc. 2nd Int. Conf. on Environmental Issues and Management of Waste in Energy and Mineral Production. 2. A.A. Balkema, Rotterdam, the Netherlands.
- Dix, R.B., P.G. Comba, and S.L. McGill. 1992. Laboratory rinsing behaviors of spent ores. p. 917-924. *In* Proc. 2nd Int. Conf. on Environmental Issues and Management of Waste in Energy and Mineral Production. 2. A.A. Balkema, Rotterdam, the Netherlands.
- Dixon, D.G. 1992. Predicting the kinetics of heap-leaching with unsteady state models. Ph.D. diss. Univ. of Nevada, Reno.
- Eching, S.O., and J.W. Hopmans. 1993a. Optimization of hydraulic functions from transient outflow and soil water pressure data. *Soil Sci. Soc. Am. J.* 57:1167-1175.
- Eching, S.O., and J.W. Hopmans. 1993b. Inverse solution of unsaturated soil hydraulic functions from transient outflow and soil water pressure data. Land, Air, and Water Resources Pap. 100021. Dep. of Land, Air, and Water Resources, Univ. of California, Davis.
- Kachanoski, R.G., E. Pringle, and A. Ward. 1992. Field measurement of solute travel times using time domain reflectometry. *Soil Sci. Soc. Am. J.* 56:47-52.
- Mallants, D., M. Vanclooster, M. Meddahi, and J. Feyen. 1994. Estimating solute transport in undisturbed soil columns using time domain reflectometry. *J. Contam. Hydrol.* 17:91-109.
- McClelland, G.E. 1991. Laboratory scale heap detoxification. *Heap and Dump Leaching Newsletter* 6:1-7.
- Murr, L.E., W.J. Schlitt, and L.M. Cathles. 1981. Experimental observations of solution flow in the leaching of copper-bearing waste. p. 271-290. *In* W.J. Schlitt (ed.) *Interfacing technologies in solution mining*. Soc. of Mining Engineers and Petroleum Engineers of AIME. Am. Inst. of Mining, Metallurgical and Petroleum Eng., New York.
- Nevada Bureau of Mines and Geology, Nevada Division of Minerals. 1997. Major mines of Nevada 1996, mineral industries in Nevada's economy. Spec. Publ. P-8. Nevada Bureau of Mines and Geology. Univ. of Nevada and Mackay School of Mines, Reno, NV.
- Parker, J.C., and M. Th. van Genuchten. 1984. Determining transport parameters from laboratory and field tracer experiments. *Virginia Agric. Exp. Stn. Bull.* 84-3.
- Rhoades, J.D., and J. van Schilfgaarde. 1976. An electrical conductivity probe for determining soil salinity. *Soil Sci. Soc. Am. J.* 40:647-651.
- Schafer, W.M., and D. Van Zyl. 1991. Cyanide degradation field study of spent heap-leach ore at the Landusky Mine. *Heap and Dump Leaching Newsletter* 6(2):1-7.
- Topp, G.C., J.L. Davis, and A.P. Annan. 1980. Electromagnetic determination of soil water content: Measurements in coaxial transmission lines. *Water Resour. Res.* 16:574-582.
- Topp, G., M. Yanuka, W. Zebchuk, and S. Zegelin. 1988. Determination of electrical conductivity using time domain reflectometry: Soil and water experiments in coaxial lines. *Water Resour. Res.* 24:945-952.
- van Genuchten, M.Th., F.J. Leij, and S.R. Yates. 1991. The RETC code for quantifying the hydraulic functions of unsaturated soils. USEPA Rep. 600/2-91/065. U.S. Salinity Laboratory, Riverside, CA.
- Zeglin, S., I. White, and D. Jenkins. 1989. Improved field probes for soil water content and electrical conductivity measurement using time domain reflectometry. *Water Resour. Res.* 25:2367-2376.